Maureen Gumbo and Gift Mehlana*

Synthesis and characterization of lanthanide MOFs based on 2,2′-bipyridine-5,5′-dicarboxylate linkers

https://doi.org/10.1515/zkri-2025-0064
Received November 9, 2025; accepted February 5, 2026;
published online February 19, 2026

Abstract: Two new metal-organic frameworks based on 2,2′-bipyridine-5,5′-dicarboxylate and lanthanide (Ln) metal ions were prepared under solvothermal conditions, using HCl as a modulator. JMS-8 and JMS-9 MOFs ($[Ln(bpdc)_3(dmf)(H_2O)_3.5dmf{\cdot}1.5H_2O]_n$) crystallised in a triclinic system with space group $P\bar{1}$. The MOFs have rod SBUs that grow along the *b*-axis. The linkers connect the SBUs along the *a*-axis and *c*-axis giving a 3D network structure. The packing diagrams show large pores as viewed on the *a*-axis and smaller pores which can be viewed on the *c*-axis. The MOFs exhibit good thermal and chemical stability. Gas sorption studies revealed low surface areas and poor CO_2 adsorption capacity.

Keywords: lanthanide MOFs; rod SBU; adsorption; buckling

1 Introduction

Metal–organic frameworks (MOFs) are a class of porous materials that have attracted significant scientific interest in recent years. Their modular construction from a wide range of inorganic metal nodes and organic linkers has enabled the rational design and synthesis of materials exhibiting unique topologies and exceptional physicochemical properties.[1] As a result, MOFs have received considerable attention owing to their broad spectrum of potential applications.[2] Structurally, MOFs are low-density crystalline materials characterized by large unit-cell volumes. They consist of metal centres linked by organic ligands through coordination bonds, forming 2D or 3D networks.[3]

The synthesis of MOFs is governed by several parameters, including temperature, concentrations of reactants, solubility of the reactants in the solvent, as well as the pH of the reaction medium.[4] Systematic variation of these parameters allows for fine control over the structural features and properties of the resulting frameworks. Furthermore, the final architecture of MOFs is influenced by factors such as the coordination geometry of the metal centres, the shape and functionality of the organic ligands, reaction pathways, choice of solvent, templates, counter-ions, and the pH of the reactive environment.[5] Several synthetic routes have been developed for MOF synthesis, including microwave-assisted, sonochemical, ionothermal, sol–gel, and microfluidic methods. Nevertheless, solvothermal and hydrothermal approaches remain the most widely employed techniques for MOF synthesis.[6–9]

The rational self-assembly strategy for the design of new MOFs has generated sustained interest due to the intriguing structural diversity of these materials and their potential as novel functional systems.[7] In MOF architectures, the inorganic component typically contributes to magnetic behaviour, mechanical robustness, and thermal stability, whereas the organic linker enhances luminescence, structural tunability, and processability.[5] Continued research efforts in this field have advanced the understanding of structure–property relationships, driven by the deliberate design and controlled synthesis of coordination polymers capable of maintaining structural integrity under elevated temperatures and pressures over extended periods.[4] The inherent high crystallinity and porosity of MOFs render them attractive for applications such as gas storage, separation, catalysis, luminescence, and drug delivery.[10] Additionally, their high surface areas and ease of functional modification make MOFs highly promising candidates for the development of advanced materials.[11] Numerous studies have demonstrated the exceptional hydrogen storage and carbon dioxide capture capabilities of MOFs at practical pressures, attributable to their high porosity, large pore volumes, and tunable internal chemical environments.[12,13]

The organic linker plays a crucial role in defining the mechanical behaviour of MOF crystals under applied physical stress.[14] When subjected to uniaxial pressure, frameworks containing linear molecular motifs may undergo

***Corresponding author: Gift Mehlana**, Faculty of Science and Technology, Department of Chemical Sciences, Midlands State University, 9055 Senga Road, Gweru, Zimbabwe, E-mail: mehlanag@staff.msu.ac.zw
Maureen Gumbo, Faculty of Science and Technology, Department of Chemical Sciences, Midlands State University, 9055 Senga Road, Gweru, Zimbabwe

buckling. At sufficiently low temperatures, such buckling phenomena can exhibit quantum mechanical characteristics, giving rise to flexibility and sensing functionalities in MOFs.[15]

In this work, two novel lanthanum–bipyridyl MOFs were synthesized, both of which clearly exhibit buckling behaviour as revealed by single crystal X-ray diffraction studies. Furthermore, the two isostructural MOFs of Ce(III) and La(III) exhibited good chemical and thermal stabilities positioning them as good candidates for catalytic applications.

2 Materials and methods

2.1 Experimental

All materials were purchased from commercial sources and were used without further purification.

2.1.1 Synthesis of JMS-8 and JMS-9 $[Ln_2(bpdc)_3(dmf)(H_2O)_3.5dmf{\cdot}1.5H_2O]_n$

2,2′-bipyridine-5,5′-dicarboxylic acid (H_2bpdc) (5.0 mg, 0.05 mmol) and 0.5 M HCl (0.25 mL) were mixed with 5 mL DMF and preheated to dissolve followed by addition of $Ln(NO_3)_3{\cdot}6H_2O$ (8.4 mg, 0.025 mmol), where Ln is La or Ce. The reaction mixture was stirred for 5 min and heated in an oven for 72 h at 60 °C. White spiky crystals of JMS-8 and yellowish spiky crystals JMS-9 were obtained. Both JMS-8 and JMS-9 were activated at 200 °C in an oven for 24 h to give JMS-8a and JMS-9a polycrystalline powders.

2.1.2 Single crystal data collection

Data collection was done on a single crystal X-ray diffraction using a Bruker KAPPA APEX II DUO diffractometer equipped with a graphite monochoromated MoKα radiation (λ = 0.71073 Å) at 173 K. Unit cell refinement and data reduction were performed using the SAINT program.[16] Data were corrected for Lorentz-polarisation and absorption effects using the multi-scan method (SADABS).[17] The structure solutions were achieved by direct methods (program SHELXS)[18] and refined anisotropically by full-matrix least-squares on F^2 using SHELXL[18,19] within the X-SEED[20] interface. The non-hydrogen atoms were located in the difference electron density maps and were refined anisotropically while all the hydrogen atoms were placed with geometric constraints and refined with isotropic temperature factors. The disordered solvent molecules were masked using the SQUEEZE program in Platon.

3 Results and discussion

MOF synthesis is based on the original models of the building-block methodology.[21,22] The subject has advanced to a point where a large diversity of framework structures are being used in numerous applications.[23,24] Thus, in addition to studies that exploit the porosity of MOFs by choice of linkers and metal centres.[25] Herein we use 2,2′-bipyridine-5,5′-dicarboxylic acid (H_2bpdc) as the linker to fabricate lanthanide MOFs based on the following factors: (i) the polydentate nature of the linker, it has of up to six donors, displaying various coordination modes; (ii) the higher symmetry of the ligand may result in ordered structures; (iii) the rigidity of the linker may decrease the possibility of lattice interpenetration in MOFs formed.[26]

3.1 Structural description

JMS-8 and JMS-9 are isostructural MOFs with La(III) and Ce(III) metal centres respectively, hence the full structural description of JMS-8 is given. Single crystal X-ray diffraction revealed the JMS-8 crystallises in a triclinic crystal system and space group $P\bar{1}$. In the asymmetric unit, we modelled two crystallographically independent La(III) metal centres coordinated to three bpdc linkers, one coordinated DMF molecule, and three coordinated water molecules. There were one and half water molecules and five DMF molecules uncoordinated in the asymmetric unit of both MOFs. In JMS-8 MOF, three of the DMF and water molecules were highly disordered, therefore a solvent mask was calculated for the disordered molecules and 277 electrons were found in a volume of 916 A^3 in 2 voids per unit cell. This is consistent with the presence of 3 DMF and 1.5 water per asymmetric unit which account for 270 electrons per unit cell. Each La(III) metal centre is coordinated to eight oxygen atoms resulting in a coordination number of 8 and a geometry of bicapped trigonal prismatic as illustrated in Figure 1a.

The structure of the JMS-8 is made up of rod secondary building units (SBU) consisting of alternating $La_2C_4O_8$ and $La_2C_2O_4$ growing along the *b*-axis (Figure 1b), the $La_2C_4O_8$ configuration of the SBU gives a paddle wheel conformation.

The bond length about the two metal centres modelled in the asymmetric unit are not the same (2.497(2) and 2.429(2) Å) and this describes why the structure has two crystallographically independent La(III) centres. The La(III) metal centres take up a geometry of bicapped trigonal prismatic.[27] The volume occupied by coordinated and uncoordinated DMF in the asymmetric unit, together with two H_2O molecules constitutes 53.6 % of the unit cell volume as estimated

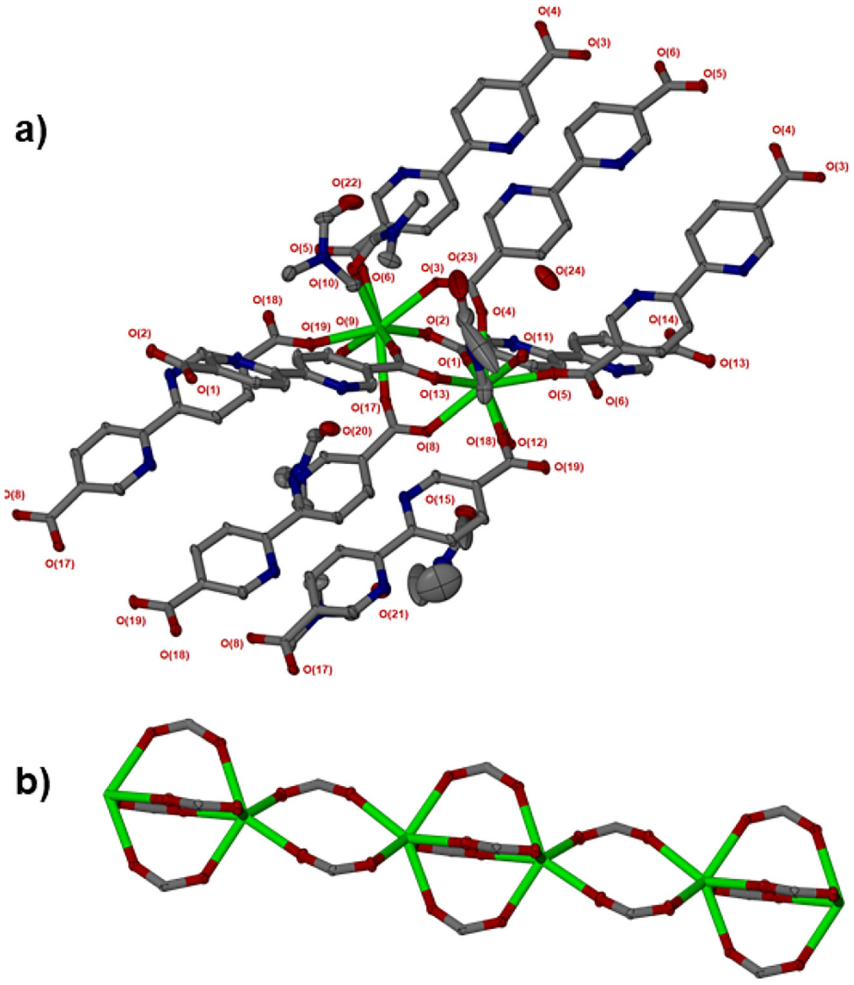

Figure 1: Connectivity of the linker to the metal ion. (a) a view of the geometry around La(III) metal centre, (b) secondary building unit of JMS-8 viewed along the *b*-axis.

in Platon[28] using a probe radius of 1.2 Å. The crystallographic information for the two isostructural MOFs is given on Table 1.

The packing diagram of JMS-8 is illustrated in Figure 2. Analysis of the structure shows the presence of both intermolecular and intramolecular hydrogen bonding that exist between coordinated water molecules and uncoordinated water and DMF molecules. This seems to strengthen the geometry and convey stability in the MOF.[27] These solvent molecules occupy the channels of 13.2 × 14.5 Å illustrated in Figure 2a.

The MOFs exhibit rod SBUs which are connected by double and single bpdc linkers which propagate along the *a*-axis and *b*-axis to give a 3D structure depicted in Figure 2a. Buckling of the linkers is observed in Figure 2a, double walled linkers buckle out interconnecting SBUs along the *b*-axis. The single walled linkers show alternating buckling in and out as the connect SBUs along the *c*-axis. The connection between SBU and the single walled linkers can be viewed along the *b*-axis (Figure 2b). A view along the *c*-axis show the slanted double walled linkers connecting to adjacent SBUs, with smaller pore which can also be seen in this axis (Figure 2c). The case of MOFs' stability, the trend is that dot < rod < sheet.[29] Hence these Rod MOFs (JMS-8a and JMS-9a), show fairly good stability.

3.2 FTIR analysis

FTIR analysis was done to provide evidence that the linkers are coordinated to the metal centres and the deprotonation of the carboxylic acid groups (Figure 3). This is consistent with what is modelled in the crystal structure.

The linker shows a carboxylic acid absorption band at 1,738 cm^{-1}, which shifts to 1,570 cm^{-1} upon MOF formation in JMS-8 (Figure 3a). This suggest that the carboxylate moiety is coordinated to the La(III) centres. A similar effect is also observed in JMS-9 (Figure 3b). Upon activation of the MOFs there is the disappearance of the absorption band at 1,652 cm^{-1} in both MOFs, confirming the successful removal

Table 1: Crystallographic and refinement parameters of JMS-8 and JMS-9.

	JMS-8	JMS-9
Empirical formula	$C_{54}H_{69}N_{12}O_{22.5}La_2$	$C_{54}H_{69}N_{12}O_{22.5}Ce_2$
Formula weight (g mol^{-1})	1,524.03	1,526.45
Temperature/K	100(2)	100(2)
Crystal system	Triclinic	Triclinic
Space group	$P\bar{1}$	$P\bar{1}$
a/Å	9.7395(6)	9.6792(7)
b/Å	14.952(9)	14.9370(10)
c/Å	22.4599(13)	22.3630(15)
α/°	79.143(2)	79.287(2)
β/°	87.953(2)	86.867(2)
γ/°	79.965(2)	81.731(2)
Volume/Å^3	3,155.24(6)	3,142.5(4)
Z	2	2
Calculated density (g/cm^3)	1.5859	1.613
μ(Mo-Kα)/mm^{-1}	15.16	15.16
F(000)	690	690
Crystal size/mm^3	0.080 × 0.120 × 0.150	0.020 × 0.080 × 0.120
Radiation	0.71073 Å	0.71073 Å
2*θ* range for data collection/°	54.99°	56.81°
Index ranges	13, 14, 15	13, 14, 15
Reflections collected	9,688	9,220
No. unique data	6,709	6,808
Goodness of fit on *S*	1.043	1.056
Final *R* indexes [$I \geq 2\sigma(I)$]	0.037	0.0300
Final wR_2 indexes [all data]	0.0953	0.0623
Largest diff peak/hole/e Å^{-3}	0.9/−1.0	0.0/−1.0

of DMF molecules. The asymmetric and symmetric carboxylate stretches in JMS-8 MOF is located at 1,570 and 1,395 cm^{-1} respectively (1,566 and 1,389 cm^{-1} in JMS-9). The band located at 1,518 cm^{-1} in JMS-8 (1,509 in JMS-9) is attributed to the C–C of the aromatic rings.

3.3 PXRD analysis

PXRD analysis shows that the calculated and experimental diffraction peaks of JMS-8 and JMS-9 are in good agreement, confirming the phase purity of the synthesized MOFs (Figure 4).

Upon activation of the MOFs to give JMS-8a and JMS-9a, it was noted that some,diffraction peaks around 10, and 16 two-theta positions disappear while the structural integrity is maintained.[21,27]

3.4 Thermal analysis

Thermal analysis of JMS-8 by TGA (Figure 5a) shows a 14 % weight loss between 26 and 133 °C which corresponds to the loss of three coordinated water molecules, and two uncoordinated DMF molecules (calculated 15 %). The 15 % weight loss between 140 and 420 °C was due to the 3 uncoordinated DMF molecule and one coordinated DMF molecule modelled in the crystal structure (calculated 17 %). There is a 2 % difference in the expected weight loss and the experimental weight loss. This was possible due to the loss of uncoordinated water molecules prior to the thermal experiment.

The TGA thermal of JMS-9 is different (Figure 5b), having a continuous weight loss of 33 % from 26 to 301 °C, corresponding to the loss of three coordinated water molecules, five uncoordinated DMF molecules and one coordinated DMF molecules (calculated 32.4 %).

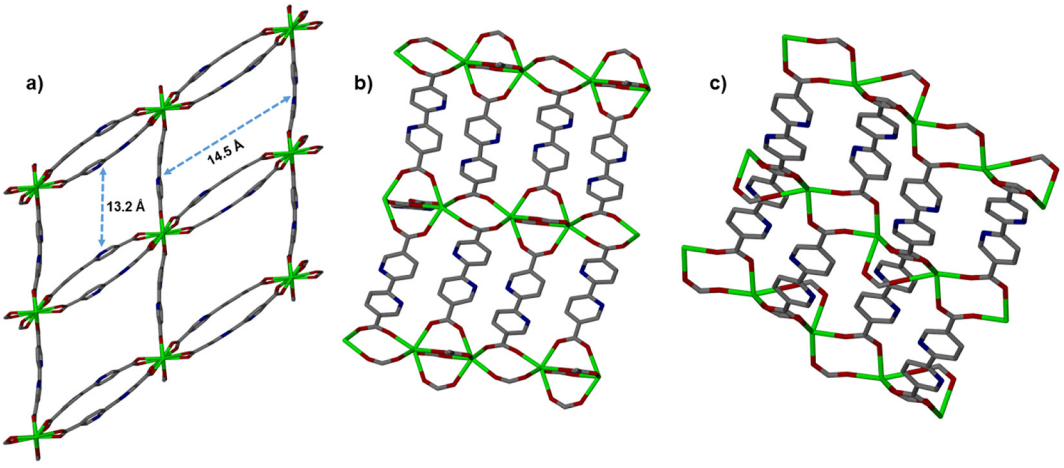

Figure 2: Packing diagram of JMS-8. (a) pores viewed along the *a*-axis, (b) MOF framework viewed along the *b*-axis, and (c) pores viewed along the *c*-axis.

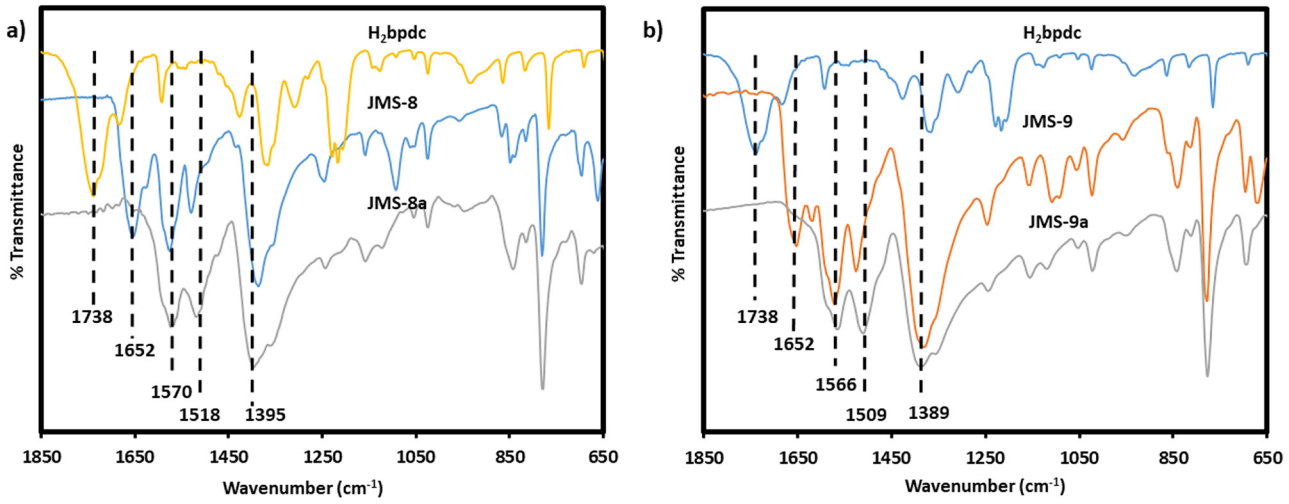

Figure 3: FTIR spectra of (a) JMS-8, (b) JMS-9.

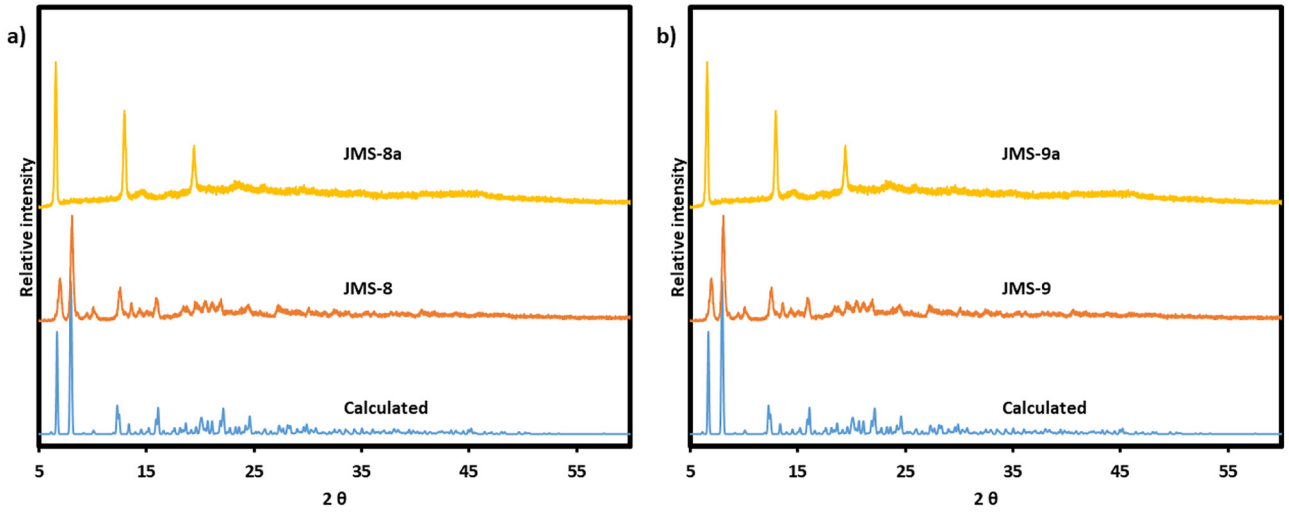

Figure 4: PXRD pattern of (a) JMS-8, (b) JMS-9.

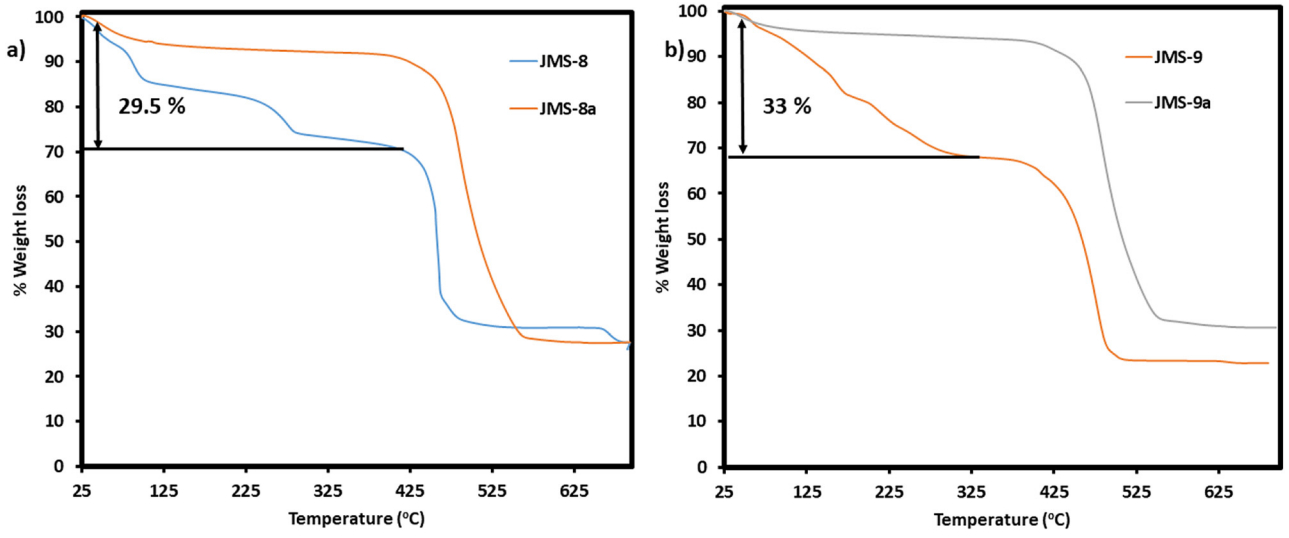

Figure 5: Thermal analysis of (a) JMS-8, (b) JMS-9.

The thermograms of both activated MOFs (JMS-8a and JMS-9a) show some weight loss below 100 °C which could be attributed to adsorption of moisture. Thermal decomposition of both the native and activated MOFs is observed above 400 °C.

3.5 Chemical stability studies of JMS-6 and JMS-7

To assess the chemical stability, the activated MOFs, **JMS-8a** and **JMS-9a** were soaked in different organic solvents for 24 h. JMS-8a and JMS-9a were soaked in methanol, ethanol, water, acetonitrile, isopropyl alcohol and THF. The recovered samples we analysed using FTIR, PXRD and TGA.

3.6 FTIR spectra of soaked materials

Successful activation of the MOFs is evidenced by the disappearance of the FTIR band at 1,652 cm^{-1}, which is attributed to the carbonyl stretch of DMF molecules.[30] FTIR studies show that the position of the asymmetric and symmetric carboxylate stretches at 1,572 and 1,395 cm^{-1} were not affected by soaking the MOFs in solvents (Figure 6). There is no evidence of the carboxylic acid absorption band at 1,738 cm^{-1}, indicating that the carboxylate sites are still coordinated to the metal centres. Both JMS-8a and JMS-9a (Figure 6) are stable is all the solvents used. Chemical stability of MOFs is important to ascertain the different working environments for the MOF materials.

3.7 PXRD diffractograms of soaked materials

PXRD shows comparable patterns of the soaked materials to the calculated pattern of the activated materials (JMS-8a and JMS-9a). This supports that the materials are stable in the solvents they were soaked in. The stability observed in the two systems may be attributed to the presence of a rod SBU and the high coordination number of the metal centre (Figure 7).

3.8 TGA curves of the soaked materials

TGA analysis revealed that the thermal stability of the MOFs is significantly reduced by soaking them in solvents, however the materials are quite stable in all the solvents used to soak them (Table 2 and Figure 8).

The activated MOFs were able to take up water and methanol molecules after the MOFs were soaked in these solvents (Table 2). Water and methanol were able to occupy the vacant pores of the MOFs due to their small molecular, mass and dimensions. Both MOFs did not show an uptake of bulky solvents such as isopropyl alcohol due to pore size restriction. The amount of THF and acetonitrile uptake per asymmetric unit was observed to be 0.5 in both JMS-8 and JMS-9. This can be attributed to similar kinetic diameters for these two molecules. JMS-9 showed more water uptake of 3.5 per asymmetric unit compared to 2.5 for JMS-8. The amount of ethanol and methanol uptake in both MOFs were comparable.

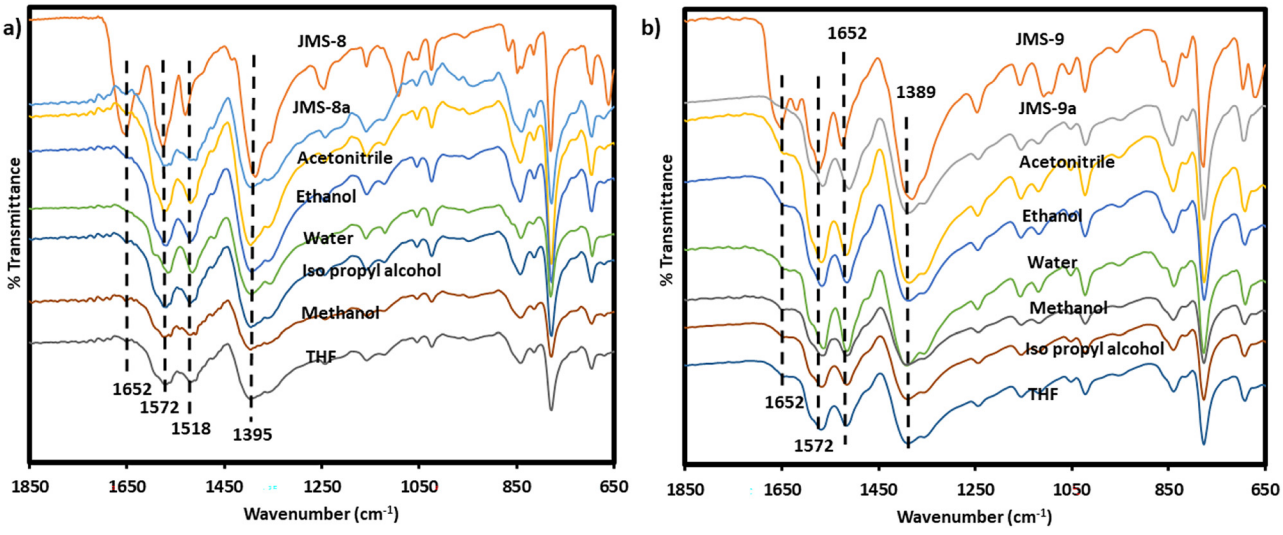

Figure 6: FTIR spectra for chemical stability studies of (a) JMS-8, (b) JMS-9 in different solvents.

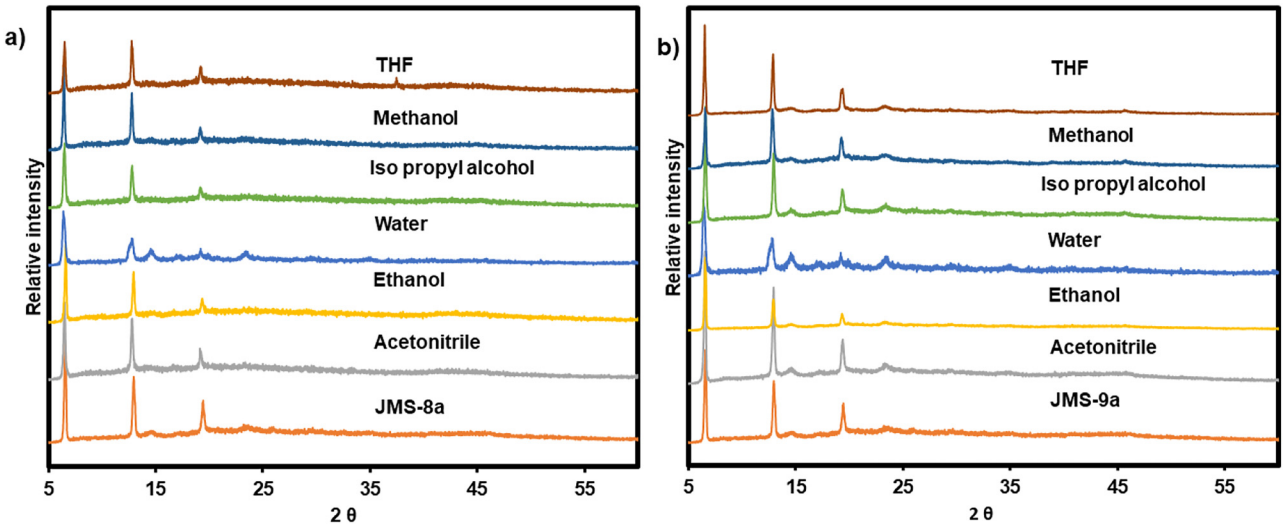

Figure 7: PXRD pattern of chemical stability studies of (a) JMS-8, (b) JMS-9.

Table 2: Solvent uptake and thermal decomposition temperature of JMS-8a and JMS-9a.

Solvent	JMS-8a		JMS-9a	
	Solvent uptake ($La_2(bpdc)_3$:sol)	Decomposition temperature (°C)	Solvent uptake ($La_2(bpdc)_3$:sol)	Decomposition temperature (°C)
Water	2.5	426	3.5	387
Methanol	3	402	2.5	402
Ethanol	1	416	1	401
Acetonitrile	0.5	436	0.5	405
Isopropyl alcohol	0	434	0	403
THF	0.5	435	0.5	401

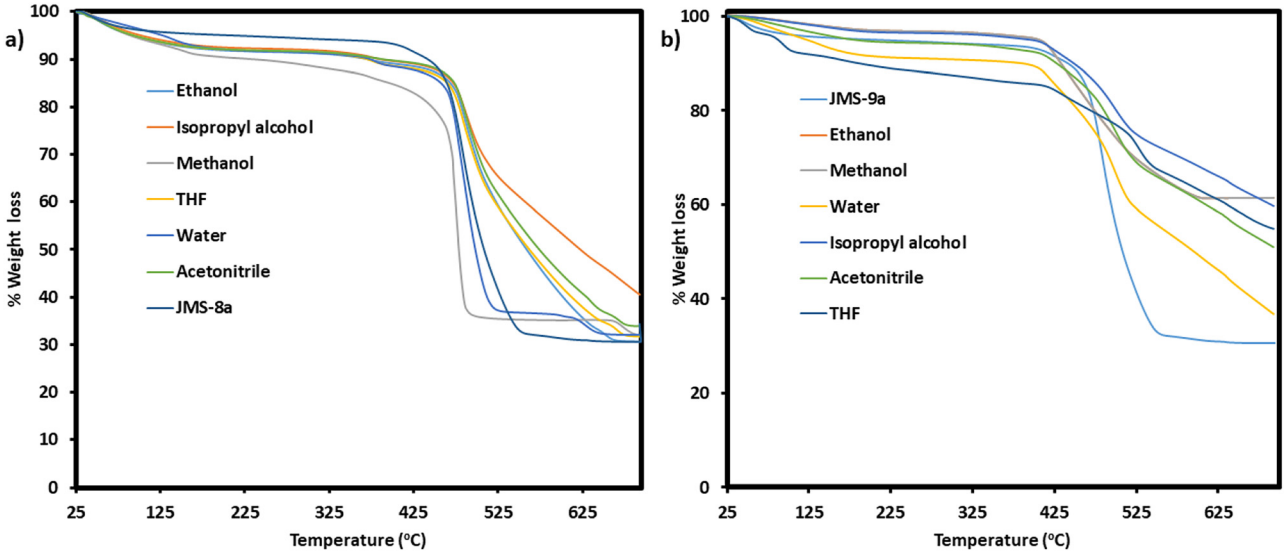

Figure 8: Thermal analysis of (a) JMS-8 and (b) JMS-9 soaked in various solvents.

The MOFs both exhibit decomposition above 400 °C in the soaked samples as compared to 420 °C in the activated material (Figure 8).

3.9 Surface characterisation

SEM analysis was used to investigative the surface morphology of the JMS-8a and JMS-9a. Both JMS-8 and JMS-9 present a rod like morphology as depicted in Figure S1. TEM studies of both JMS-8a and JMS-9a were done to check the morphology of the MOFs. As illustrated in Figure S2, both MOFs exhibits a block morphology. EDX studies was used to further confirm the presence of desired elements and to check possible presence of impurities. EDX can detect numerous elements, even those with low atomic number. Pristine JMS-8a and JMS-9a MOFs only contained lanthanum metal, carbon, nitrogen and oxygen atoms (Figure S3). Elementary mapping was employed to study the distribution of the different elements present in the JMS-8 and JMS-9 MOF matrix. As illustrated in Figure S4, the Ln metals are evenly distributed within the MOF matrix. BET analysis was done to conform the surface area and pore size distribution of the JMS-8 (Figure S5). The MOF shows at type 1 adsorption isotherm and a surface area of 20 cm^2/g. The pore size distribution shows a greater degree of micro porosity, which is characteristics of regular MOFs. CO_2 sorption of the materials studies were attempted; however, the materials did not show good CO_2 sorption properties.

4 Conclusions

Two isostructural MOFs JMS-8 and JMS-9 were reported. These MOFs were analysed by diffraction and spectroscopic methods. The activated phases JMS-8a and JMS-9a were exposed to ethanol, methanol, water, acetonitrile, isopropyl alcohol and THF to test their chemical stability. Both MOFs show good chemical and thermal stability. Gas sorption studies however, show that the MOFs have very low surface areas as well as poor CO_2 sorption. Owing to the thermal and chemical stability, future work will focus on encapsulating molecular catalysts in both MOFs CO_2 hydrogenation studies.

Acknowledgments: This document has been produced with the financial assistance of the European Union (Grant no. DCI-PANAF/2020/420-028), through the African Research Initiative for Scientific Excellence (ARISE), pilot programme. ARISE is implemented by the African Academy of Sciences with support from the European Commission and the African Union Commission. The contents of this document are the sole responsibility of the author(s) and can under no circumstances be regarded as reflecting the position of the European Union, the African Academy of Sciences, and the African Union Commission.

Research ethics: Not applicable.

Informed consent: Not applicable.

Author contributions: All authors have accepted responsibility for the entire content of this manuscript and approved its submission. Maureen Gumbo was responsible for experimental work and drafting of the manuscript. Gift Mehlana was responsible for editing the manuscript.

Use of Large Language Models, AI and Machine Learning Tools: None declared.

Conflict of interest: The authors state no conflict of interest.

Research funding: European Union (Grant no. DCI-PANAF/2020/420-028).

Data availability: Not applicable.

References

1. Shi, Y.; Yang, A. F.; Cao, C. S.; Zhao, B. Applications of MOFs: Recent Advances in Photocatalytic Hydrogen Production from Water. *Coord. Chem. Rev.* **2019**, *390*, 50–75.
2. Smaldone, R. A.; Forgan, R. S.; Furukawa, H.; Gassensmith, J. J.; Slawin, A. M. Z.; Yaghi, O. M.; Stoddart, J. F. Metalorganic Frameworks from Edible Natural Products. *Angew. Chem., Int. Ed.* **2010**, *49* (46), 8630–8634.
3. Yang, D.; Gates, B. C. Catalysis by Metal Organic Frameworks: Perspective and Suggestions for Future Research. *ACS Catal.* **2019**, *9*, 1779–1798.
4. Verma, A.; Purkait, M. K. Synthesis, Characterization and Physical Properties Studies of an Anionic Surfactant. *Indian J. Chem. Technol*. **2010**, *17* (3), 233–237.
5. Liu, B.; Fernandes, J. A.; Tomé, J. P. C.; Almeida, P. F. A.; Cunha-Silva, L. Multidimensional Transition Metal Complexes Based on 3-Amino-1H-1,2,4-Triazole-5-Carboxylic Acid: From Discrete Mononuclear Complexes to Layered Materials. *Molecules* **2015**, *20* (7), 12341–12363.
6. Makuve, N.; Darkwa, J.; Mehlana, G.; Makhubela, B. C. E. Hydrogenation of Carbon Dioxide to Formate Using a Cadmium-Based Metal–Organic Framework Impregnated with Nanoparticles. *Inorganics* **2022**, *10* (3). https://doi.org/10.3390/inorganics10030030.
7. Pachfule, P.; Dey, C.; Panda, T.; Banerjee, R. Synthesis and Structural Comparisons of Five New Fluorinated Metal Organic Frameworks (F-MOFs). *CrystEngComm* **2010**, *12* (5), 1600–1609.
8. Olayemi, V. T.; Tella, A. C.; Adekola, F. A.; Clayton, H. S.; Oladipo, A. C.; Mehlana, G.; Adeniyi, S. O.; Oluwatobi, S. O.; Joseph, O. O.; Stephen, P. A.; Mokaya, R. A Co-Crystallised Cobalt(II) Cluster of Pyridinedicarboxylic Acid (PDC) as a Luminescent Material for Selective Sensing of Methanol. *J. Fluoresc.* **2021**, *31* (4), 1177–1190.
9. Marazani, L. G.; Gascon-Perez, V.; Pathak, A.; Tricarico, M.; Tan, J. C.; Zaworotko, M. J.; Makhubela, B. C. E.; Mehlana, G. Water Sorption Studies with Mesoporous Multivariate Monoliths Based on UiO-66. *Mater. Adv.* **2024**, *5* (19), 7679–7689.
10. Liu, C. B.; Li, Q.; Wang, X.; Che, G. B.; Zhang, X. J. A Series of Lanthanide (III) Coordination Polymers Derived via in Situ Hydrothermal

Decarboxylation of Quinoline-2,3-Dicarboxylic Acid. *Inorg. Chem. Commun*. **2014**, *39*, 56–60.
11. Zati-Hanani, S.; Adnan, R.; Latip, A. F. A.; Sipaut, C. S. Synthesis, Characterization and Thermal Properties of Two Novel Lanthanide 2,2′-Biquinoline-4,4′-Dicarboxylate Complexes. *Sains Malays.* **2011**, *40* (9), 999–1006.
12. Dong, X.; Liu, X.; Chen, Y.; Zhang, M. Screening of Bimetallic M-Cu-BTC MOFs for CO2 Activation and Mechanistic Study of CO2 Hydrogenation to Formic Acid: A DFT Study. *J. CO2 Util.* **2018**, *24*, 64–72.
13. Liu, J.; Li, Z.; Zhang, X.; Otake, K. I.; Zhang, L.; Peters, A. W.; Young, M. J.; Bedford, N. M.; Letourneau, S. P.; Mandia, D. J.; Elam, J. W.; Farha, O. K.; Hupp, J. T. Introducing Nonstructural Ligands to Zirconia-Like Metal-Organic Framework Nodes to Tune the Activity of Node-Supported Nickel Catalysts for Ethylene Hydrogenation. *ACS Catal.* **2019**, *9* (4), 3198–3207.
14. Ying, P.; Zhang, J.; Zhong, Z. Pressure-Induced Phase Transition of Isoreticular MOFs: Mechanical Instability Due to Ligand Buckling. *Microporous Mesoporous Mater*. **2021**, *312*, 110765.
15. Geilhufe, R. M. Quantum Buckling in Metal–Organic Framework Materials. *Nano Lett.* **2021**, *21* (24), 10341–10345.
16. Saint. Version 7.60a; Bruker AXS Inc: Madison, WI, USA, 2006.
17. Sheldrick, G. M. *Acta Crystallogr.* **2015**, *C71*, 3–8.
18. Sheldrick, G. M. A Short History of Shelx. *Acta Crystallogr., Sect. A: Found. Crystallogr.* **2008**, *64*, 112–122.
19. Sheldrick, G. M. Alphabetical List of Shelxl Instructions [Internet], Vol. *11*, 2014. http://shelx.uni-ac.gwdg.de/SHELX/shelxl_comlist.pdf.
20. Barbour, L. J. X-Seed: A Software Tool for Supramolecular Crystallography. *J. Supramol. Chem.* **2001**, *1*, 189–191.
21. Hungwe, J.; Tshuma, P.; Gumbo, M.; Noa, F. M. A.; Öhrström, L.; Mehlana, G. Tuning the Topology of a 2D Metal-Organic Framework from 2D to 3D Using Modulator Assisted Synthesis. *CrystEngComm* **2023**, *25* (10), 1486–1494.
22. Reade, T. J.; Murphy, T. S.; Calladine, J. A.; Horvath, R.; Clark, I. P.; Greetham, G. M.; Towrie, M.; Lewis, W.; George, M. W.; Champness, N. R. Photochemistry of Framework-Supported M(diimine)(CO)3X Complexes in Three-Dimensional Lithium Carboxylate Metal-Organic Frameworks: Monitoring the Effect of Framework Cations. *Philos. Trans. A Math. Phys. Eng. Sci.* **2017**, *375* (2084). https://doi.org/10.1098/rsta.2016.0033.
23. Tshuma, P.; Makhubela, B. C. E.; Bingwa, N.; Mehlana, G. Palladium(II) Immobilized on Metal-Organic Frameworks for Catalytic Conversion of Carbon Dioxide to Formate. *Inorg. Chem*. **2020**, *59* (10), 6717–6728.
24. Strauss, I.; Chakarova, K.; Mundstock, A.; Mihaylov, M.; Hadjiivanov, K.; Guschanski, N.; Caro, J. UiO-66 and UiO-66-NH2 Based Sensors: Dielectric and FTIR Investigations on the Effect of CO2 Adsorption. *Microporous Mesoporous Mater.* **2020**, *302*, 110227.
25. Feng, L.; Yuan, S.; Zhang, L. L.; Tan, K.; Li, J. L.; Kirchon, A.; Liu, L. M.; Zhang, P.; Han, Y.; Chabal, Y. J.; Zhou, H. C. Creating Hierarchical Pores by Controlled Linker Thermolysis in Multivariate Metal-Organic Frameworks. *J. Am. Chem. Soc.* **2018**, *140* (6), 2363–2372.
26. Fang, M.; Wang, T.; Lu, X.; Song, A.; Shen, L.; Tian, H. Two 3-d Metal Organic Frameworks Containing 2,2′-Bipyridine-5,5′-Dicarboxylic Acid: Synthesis, Structure, and Magnetic Properties. *J. Coord. Chem*. **2014**, *67* (13), 2280–2286.
27. Tshuma, P.; Makhubela, B. C. E.; Ndamyabera, C. A.; Bourne, S. A.; Mehlana, G. Synthesis and Characterization of 2D Metal-Organic Frameworks for Adsorption of Carbon Dioxide and Hydrogen. *Front. Chem.* **2020**, *8*, 1–11.
28. Spek, A. L. Single-Crystal Structure Validation with the Program Platon. *J. Appl. Crystallogr.* **2003**, *36*, 7–13.
29. Amombo Noa, F. M.; Abrahamsson, M.; Ahlberg, E.; Cheung, O.; Göb, C. R.; McKenzie, C. J.; Öhrström, L. A Unified Topology Approach to Dot-Rod- and Sheet-MOFs. *Chem* **2021**, *7* (9), 2491–2512.
30. Mehlana, G.; Bourne, S. A.; Ramon, G.; Öhrström, L. Concomitant Metal Organic Frameworks of Cobalt(II) and 3-(4-Pyridyl) Benzoate: Optimized Synthetic Conditions of Solvatochromic and Thermochromic Systems. *Cryst. Growth Des*. **2013**, *13* (2), 633–644.

Supplementary Material: This article contains supplementary material (https://doi.org/10.1515/zkri-2025-0064).